Control Strategies for Formation Flight in the Vicinity of the Libration Points

B. G. Marchand and K. C. Howell

Reprinted from

Journal of Guidance, Control, and Dynamics

Volume 28, Number 6, Pages 1210-1219

A publication of the
American Institute of Aeronautics and Astronautics, Inc.
1801 Alexander Bell Drive, Suite 500
Reston, VA 20191-4344

JOURNAL OF GUIDANCE, CONTROL, AND DYNAMICS
Vol. 28, No. 6, November–December 2005

Control Strategies for Formation Flight in the Vicinity of the Libration Points

B. G. Marchand* and K. C. Howell†
Purdue University, West Lafayette, Indiana 47907

The concept of formation flight of multiple spacecraft offers many promising possibilities, both for space exploration and the associated technology development. Past studies on formation flight have focused primarily on Earth-orbiting clusters. However, space-based observatory and interferometry missions, such as the proposed Terrestrial Planet Finder and the Micro Arcsecond X-ray Imaging Mission, reflect plans for formation flight in multibody regimes, particularly in the vicinity of the sun–Earth/moon libration points. Two specific tasks are accomplished in this study. First, in a dynamically sensitive regime such as that near the libration points, baseline propulsive requirements are established. A decentralized control strategy based on existing linear and nonlinear control techniques is employed and the results are presented through a series of sample mission configurations. Note that the control problem is formulated to facilitate future tradeoff studies in the libration point environment. The analysis is presented within the context of both the circular restricted three-body problem and the more complete ephemeris model. Once baseline costs are available, the second task is the introduction of potential constraints. These constraints may affect not only the formation control strategies but also the conceptual design of the mission, and their influence on the cost is evaluated.

Introduction

A MULTISPACECRAFT formation refers to a distributed measurement system comprising two or more spacecraft. Formation flight, then, implies that each spacecraft is controlled to maintain a prespecified configuration relative to the other vehicles in the formation. This may require that the individual vehicles maintain a constant relative distance, and perhaps orientation, over a specified period of time. In addition, the formation-keeping goals may also require multiple reorientations or reconfigurations during the lifetime of a mission. In general, such constraints are not likely to be consistent with the natural dynamics in either the two-body problem (2BP) or a multibody regime; thus, a control strategy is required. Much of the research to date refers to the control of constellations, clusters, and formations for Earth-orbiting missions.[1–17] In this case, the influence of other gravitational perturbations can often be safely ignored as an initial approximation. However, recent interest in formation flight near the sun–Earth/moon (SEM) libration points requires an assessment of the effectiveness of the more commonly implemented control techniques. The nature of the dynamic force model in this region of space does not allow an analytical solution for the reference. Although some approximations are available, any analysis involving formation flight in multibody systems is still strongly dependent on numerical methods.

In the two-body regime, optimal control techniques are those most commonly encountered in the available literature on formation flight.[1–10] Many of these references include the reasonable assumption that the vehicle separations are relatively small. Hence, the reference motion is modeled completely in terms of the linearized dynamics, as described by the Clohessy–Wiltshire equations in the 2BP. The controller is then applied to the linear system, though its effectiveness in the nonlinear model may not be explicitly demonstrated. Impulsive control schemes are also often implemented but are only applicable to formations that do not require precise tracking of a reference solution.[11–13] This approach is usually based on a Keplerian formulation of the two-body dynamics. Nonlinear methods, such as Lyapunov-based control,[14,15] combined with adaptive control methods,[16,17] are successfully applied to small formations in the two-body regime. Among these researchers, only de Queiroz et al.[16] and Yan et al.[17] develop their control strategies based solely on the full nonlinear equations of motion.

Recent interest in formations that evolve near the vicinity of the SEM libration points has inspired a growing number of studies regarding formation-keeping in the three-body problem. Among these, Scheeres and Vinh[18] identify a nontraditional yet innovative control law that achieves bounded motion near the vicinity of a halo orbit, as determined in Hill's model. Although the latter approach is not suitable for precise formation-keeping, nor is it necessarily the optimal way to achieve boundedness, it does satisfy other goals that may be important for certain types of missions. In particular, the natural winding frequency of the spacecraft around the reference halo orbit is significantly increased. This is consistent with one of the stated requirements for the Terrestrial Planet Finder (TPF) mission,[19] where the formation is required to achieve a particular rotation rate that is not consistent with the natural dynamics near this region of space.

Formations modeled in the circular restricted three-body problem (CR3BP) represent a good starting point. However, ultimately, any definitive formation-keeping studies must be performed in the n-body ephemeris model. In this model, the time invariance properties of the CR3BP are lost and, consequently, precisely periodic orbits do not exist near the libration points. Within the framework of the ephemeris model, Hamilton[20] and Folta et al.[21] consider linear optimal control for formation flight relative to Lissajous trajectories, as determined in the ephemeris model. However, the evolution of the controlled formation is approximated from a linear dynamic model relative to the integrated reference orbit.

Other formation control studies, associated with the ephemeris model, are based on a dynamical systems approach. The initial focus of these investigations is the determination of the natural formation dynamics on the center manifold near the libration points. Initially, Howell and Barden[22–24] investigated formation flying in the perturbed SEM system. Later studies by Howell and Marchand[25] further explored the natural formation dynamics along the center manifold. Howell and Barden use the system dynamics to capture a naturally occurring six-satellite formation near L_1 or L_2. Further analyses consider strategies to maintain a planar formation of the six vehicles in an orbit about the sun–Earth L_1 point,[23,24] that is, controlling

Received 21 May 2004; revision received 5 February 2005; accepted for publication 5 February 2005.

*Ph.D. Candidate, School of Aeronautics and Astronautics. Student Member AIAA.

†Professor, School of Aeronautics and Astronautics. Associate Fellow AIAA.

spherical and aspherical configurations. In that regard, the analysis presented here is applicable regardless of the working frame, inertial or rotating.

Control strategies that rely on the linearized dynamics, such as LQR, require that a nominal formation-keeping cost $\boldsymbol{u}_d(t)^\circ$ be initially determined. Of course, in the end, the net control effort is the sum of this nominal cost and the differential cost determined via the LQR approach. One advantage of feedback linearization methods is that the explicit determination of nominal costs is unnecessary because everything can be accomplished in one step. Regardless of the control approach, a detailed study of the nominal formation-keeping costs is necessary to establish baseline requirements to support the design of the onboard propulsion system characteristics. In the case of formation flight near the libration points, the results of this study indicate that, depending on the dynamic constraints imposed by a particular mission, the propulsive requirements may approach lower limits that are challenging. These seemingly insignificant thrust levels, however, are still essential for precision formation flight.

Fixed-State Formations Relative to the Rotating Frame

One possible type of formation corresponds to a configuration such that the relative distance between the chief-spacecraft and the deputy is constant and the relative orientation of the chief–deputy line is fixed with respect to the rotating frame R. Suppose that differential equations (2) are associated with an inertial reference frame. Furthermore, assume that the position and velocity state elements are measured in terms of inertial coordinates. Let $\boldsymbol{\rho}_R$ represent a relative position vector, initially defined in terms of rotating frame coordinates, such that $\boldsymbol{r}_d = \boldsymbol{r}_c + \boldsymbol{\rho}_R$. If the nominal motion requires that $\boldsymbol{\rho}_R$ be fixed in the rotating frame, then ${}^R\dot{\boldsymbol{\rho}}_R = {}^R\mathrm{d}\boldsymbol{\rho}_R/\mathrm{d}t = \boldsymbol{0}$. In terms of inertial coordinates, the nominal motion can then be expressed as $\boldsymbol{\rho}_I = \{{}^IC^R\}\boldsymbol{\rho}_R$ and ${}^I\dot{\boldsymbol{\rho}}_I = \{{}^IC^R\}[{}^I\boldsymbol{\omega}^R \times \boldsymbol{\rho}_R]$, where ${}^I\boldsymbol{\omega}^R = \dot{\theta}\hat{\boldsymbol{z}}$ describes the rotation rate of frame R relative to frame I, and $\{{}^IC^R\}$ represents the associated 3×3 coordinate transformation matrix between the inertial and rotating frames. Substitution of these constraints into Eq. (2), for $\boldsymbol{u}_c(t) = \boldsymbol{0}$, indicates that the nominal control input required to enforce a constant distance and spatial orientation in the rotating frame is evaluated as

$$\boldsymbol{u}_d(t)^\circ = \{{}^IC^R\}\left[{}^I\dot{\boldsymbol{\omega}}^R \times \boldsymbol{\rho}_R + {}^I\boldsymbol{\omega}^R \times \left({}^I\boldsymbol{\omega}^R \times \boldsymbol{\rho}_R\right)\right] - \Delta\boldsymbol{f}(\boldsymbol{r}^\circ, \boldsymbol{r}_c) \tag{3}$$

Note that, in the CR3BP, ${}^I\boldsymbol{\omega}^R$ is constant and, hence, ${}^I\dot{\boldsymbol{\omega}}^R = {}^R\mathrm{d}{}^I\boldsymbol{\omega}^R/\mathrm{d}t = \boldsymbol{0}$. However, in the ephemeris model, the nominal control effort is defined as written in Eq. (3). The quantities ${}^I\boldsymbol{\omega}^R$ and ${}^I\dot{\boldsymbol{\omega}}^R$ are approximated directly from the available planetary ephemeris.

To develop a general sense of the formation-keeping costs associated with this type of nominal motion, first consider the problem within the context of the CR3BP. In this model, the trajectory of the chief spacecraft is assumed to evolve along a natural periodic halo orbit and completes one revolution in approximately six months. A single deputy spacecraft, then, is located at a specific distance (ρ) and orientation (ξ, β) relative to the chief, as illustrated in Fig. 1. This is defined as the baseline formation. Formation-keeping costs can be assessed in a variety of ways. Often, cost is represented as the integral ΔV of the norm of the applied control input over the duration of the mission. In the present example, however, the formation-keeping cost, illustrated in Fig. 2, is determined in terms of the mean control acceleration over 180 days; that is, one revolution along the path of the chief spacecraft. Three surfaces are displayed in Fig. 2. The narrower green surface corresponds to a halo orbit characterized by a 1.2×10^6 km maximum out-of-plane amplitude (A_z), the intermediate blue contour is associated with an A_z amplitude of 700,000 km, and the wider red outline represents the results for an A_z amplitude of 200,000 km. Each surface is associated with a formation defined by a 5000-km separation (ρ). The formation-keeping cost, then, is represented as a function of the azimuth (ξ) and elevation (β) of the chief–deputy line, as defined in Fig. 1.

The cost range in Fig. 2 indicates that, for a 1000-kg spacecraft, thrust levels on the order of 0.5 to 2 mN are necessary to enforce a 5000-km formation that is fixed in the rotating frame. This is equivalent to 10 m/s $< \Delta V <$ 30 m/s, via continuous thrust, over 180 days. The specified thrust levels, for this particular example, are certainly deliverable based on the propulsion systems available today. However, the numerical evidence suggests that the relation between the formation-keeping cost and the nominal relative separation is roughly linear. That is, if the nominal separation decreases by one order of magnitude then the cost also decreases by one order of magnitude. Hence, if the nominal relative separations are on the order of a few meters, then the required thrust levels can be on the order of 10^{-9}–10^{-12} N. Although these thrust levels may appear negligible, if submillimeter tracking accuracy is required, these control inputs cannot be neglected. Even if technological developments allow for thrust delivery in this range, the error levels may potentially be on the same order of magnitude as the nominal thrust itself. Given the dynamic sensitivities of this model, as well as all other uncertainties present in a real system, precision formation-keeping, in the submillimeter range, may be challenging.

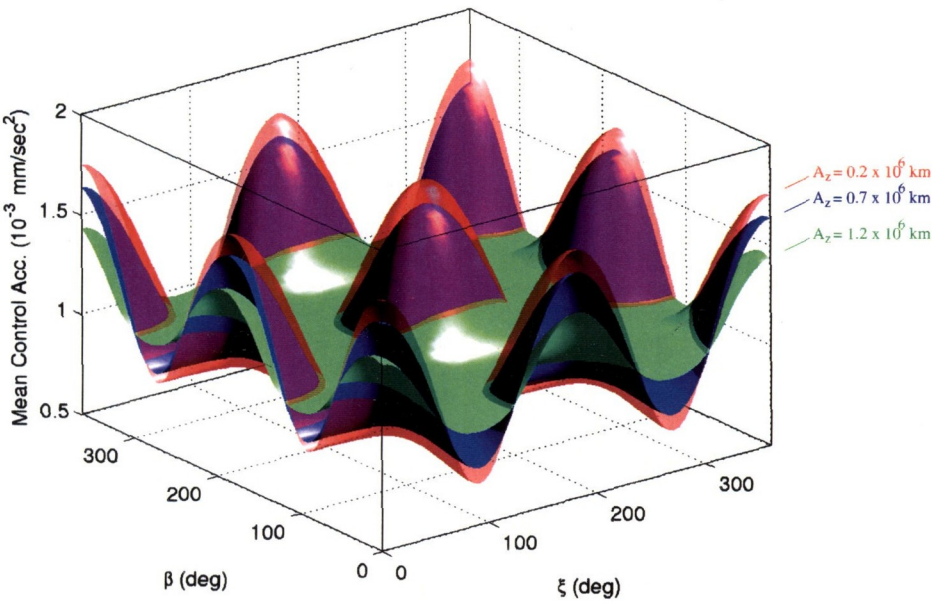

Fig. 2 Nominal formation-keeping cost associated with various 5000-km formations, fixed relative to the rotating frame (over 6 months); each surface is associated with a particular L_1 halo orbit ($A_z = 2 \times 10^5, 7 \times 10^5$, and 1.2×10^6 km).

It is important to note that the cost trends in Fig. 2 are influenced by the size of the reference orbit of the chief spacecraft. In fact, the formation-keeping cost increases nonlinearly as the amplitude of the reference orbit increases. It is also evident from Fig. 2 that formations orthogonal to the SEM line result in the lowest formation-keeping costs. The maximum cost, then, corresponds to a formation that is always parallel to the SEM line. A thorough numerical analysis, over a large section of the L_1 and L_2 halo families, reveals that this trend holds as long as $A_z < 1.55 \times 10^6$ km. Above this range, the formation-keeping costs become prohibitive regardless of the nominal configuration.

Fixed-State Formations Relative to the Inertial Frame

A formation that is fixed with respect to the inertial frame (I) must satisfy $\boldsymbol{r}_d(t) = \boldsymbol{\rho}_I$ such that $\boldsymbol{\rho}_I$ is constant and ${}^I\dot{\boldsymbol{\rho}}_I = {}^I\ddot{\boldsymbol{\rho}}_I = \boldsymbol{0}$. Note that the subscript I implies that the measure numbers of $\boldsymbol{\rho}_I$ are associated with the inertial frame. The nominal control input necessary to enforce this particular configuration, as determined from Eq. (2), is expressed as

$$\boldsymbol{u}_d(t)^\circ = -\Delta \boldsymbol{f}(\boldsymbol{r}^\circ, \boldsymbol{r}_c) \tag{4}$$

For a 5000-km nominal separation, a cost analysis, similar to that performed in the preceding example, reveals that the formation-keeping costs are not significantly affected by holding the formation fixed relative to the inertial frame. Numerical evidence does indicate, however, that the nominal orientations associated with the minimum and maximum cost configurations, in this case, do change.

Formation Control

In this study, linear optimal control is compared to input-state and input/output feedback linearization methods. The mathematical development, and subsequent computational implementation, associated with feedback linearization methods is simpler than that corresponding to an optimal control strategy. However, in contrast to an LQR approach, the physical implementation of an onboard nonlinear control law, such as that presented here, may introduce additional issues, as discussed by Chen et al.[30] This is particularly true for highly nonlinear dynamics such as those associated with the n-body problem. However, from a computational perspective, feedback linearization techniques are extremely useful as a preliminary analysis tool when compared to optimal control methods. This allows for more comprehensive studies over a wide variety of mission scenarios while preserving the reliability of the results.

Input-State and Input/Output Feedback Linearization

Feedback linearization, as discussed by Slotine and Li,[31] is a nonlinear control strategy that allows the designer to prespecify the desired response characteristics while achieving the tracking goals. In input-state feedback linearization, here termed input feedback linearization (IFL), this is accomplished first by applying an input that cancels the nonlinear terms in the equations of motion. A second term is subsequently added such that the desired error response characteristics are satisfied. Although canceling the nonlinear terms may generally lead to prohibitive control inputs, the dynamic sensitivity characteristic of the region of space near the libration points creates an environment well suited to this particular approach. Of course, any form of feedback linearization requires full-state feedback, one of the disadvantages of the approach. However, for formation flight, if accurate relative state information is available, this method can be a powerful tool at the preliminary design stage.

To illustrate the basic concept of IFL control, consider the equations of motion in Eq. (2). It is possible to select $\boldsymbol{u}_d(t)$ such that the state follows a critically damped error response that meets some prescribed settling time requirement. For instance, let the response be characterized by a natural frequency ω_n. Then the following control law achieves the desired response characteristics and converges onto the prescribed nominal path; that is,

$$\boldsymbol{u}_d(t) = \ddot{\boldsymbol{r}}^\circ - 2\omega_n(\dot{\boldsymbol{r}} - \dot{\boldsymbol{r}}^\circ) - \omega_n^2(\boldsymbol{r} - \boldsymbol{r}^\circ) - \Delta \boldsymbol{f} \tag{5}$$

The last term in Eq. (5) effectively cancels the nonlinear terms due to gravity and SRP; the first three terms force the response to follow the desired error response and track the nominal path. An acceptable response is arbitrarily selected as one that reaches the desired solution within a day—assuming the position injection errors are not unreasonably large. A nondimensional angular frequency (ω_n) of at least 1000 meets this requirement. It should be noted that decoupling the states is not necessarily the "optimal" solution; it is simply a way to accomplish the task. Furthermore, this approach is useful when the formation requires that both distance and orientation be completely specified in time. However, in formation flight applications, it may not be necessary to track each state individually. If the formation only requires that relative distance, or some other function of the state variables, be specified, then input/output feedback linearization is better suited for the task.

Input/output feedback linearization, here termed output feedback linearization (OFL), is similar in concept to the IFL approach. However, instead of designing a control law that tracks a specified state, the control law is determined to track a nonlinear function of the state variables. For instance, let $\boldsymbol{H}(\boldsymbol{r}, \dot{\boldsymbol{r}})$ represent a nonlinear vector function that depends on the relative state of the deputy. Note that this function does not depend explicitly on the control input $\boldsymbol{u}_d(t)$. The goal, then, is to identify $\boldsymbol{u}_d(t)$ such that $\boldsymbol{H}(\boldsymbol{r}, \dot{\boldsymbol{r}}) \rightarrow \boldsymbol{H}^\circ$, where $\boldsymbol{H}^\circ$ represents the nominal value of $\boldsymbol{H}(\boldsymbol{r}, \dot{\boldsymbol{r}})$. To do this, the function $\boldsymbol{H}(\boldsymbol{r}, \dot{\boldsymbol{r}})$ is differentiated with respect to time until the control input appears explicitly in the resulting expression. Once the input appears, it may be possible to identify at least one solution that satisfies the tracking goal. The number of solutions available depends on the dimension of the vector function $\boldsymbol{H}(\boldsymbol{r}, \dot{\boldsymbol{r}})$ and the number of available control inputs.

LQR and Feedback Linearization

In the n-body problem, an LQR—as derived for linear time-varying systems—requires the solution of a two-point boundary-value problem with mixed boundary conditions. More specifically, the nominal trajectory must first be numerically integrated, because no analytical solution is available, and then stored for the controller gain matrix to be determined. The determination of the gain matrix requires a second numerical integration that depends on the availability of the results from the first integration. Finally, the controller can be applied to a perturbed trajectory, during a third integration, by accessing or approximating the stored gain matrix elements as necessary.

For systems that are invariant under time transformation, such as the CR3BP, it is possible to reduce the optimal two-point boundary-value problem to an initial-value problem, as demonstrated by Howell and Marchand.[32] Although this transformation simplifies the implementation of the controller in the CR3BP, ultimately an actual mission requires that this analysis be performed in the general ephemeris model, with no assumptions about the motion of the primaries. Unlike the CR3BP, the ephemeris model is not invariant under time transformation. Hence, implementing an LQR in the ephemeris model, once again, requires the solution of a two-point boundary-value problem. This can be a very computationally intensive problem, especially when multiple deputy vehicles with different nominal paths are considered.

As suggested by the results of the present investigation, it is possible to select the design parameters such that the IFL and LQR controllers yield similar response characteristics at almost identical costs. However, as previously noted, the input-state feedback approach is determined to be the most computationally efficient of the two methods from a preliminary design perspective. In contrast to the IFL approach, OFL allows for the greatest flexibility because it is possible to specify the error response for functions of the state variables rather than the state variables themselves. Ultimately, all of these methods are, of course, effective in accomplishing the formation-keeping goals. The method selected is a matter of choice and the stage of the analysis.

Application of Input/Output Feedback Linearization to Spherical Formations

As previously mentioned, the OFL approach allows for the determination of a control law that forces a vector function of the state

Table 1 OFL control of spherical formations

Formulation	Control law
$\frac{d^2r}{dt^2} \rightarrow$	$\boldsymbol{u}_d(t) = \left\{r\left[-2\omega_n\dot{r} - \omega_n^2(r - r^\circ)\right] + \dot{r}^2 - (\dot{\boldsymbol{r}}\cdot\dot{\boldsymbol{r}}) - (\Delta\boldsymbol{f}\cdot\boldsymbol{r})\right\}\left(\frac{\boldsymbol{r}}{r^2}\right)$
$\frac{d^2r}{dt^2} \rightarrow$	$\boldsymbol{u}_d(t) = \left\{\frac{\left[-2\omega_n\dot{r} - \omega_n^2(r - r^\circ)\right]}{r} - \frac{(\dot{\boldsymbol{r}}\cdot\dot{\boldsymbol{r}})}{r^2}\right\}\boldsymbol{r} + \left(\frac{\dot{r}}{r}\right)\dot{\boldsymbol{r}} - \Delta\boldsymbol{f}$
$\frac{d^2(r^2)}{dt^2} \rightarrow$	$\boldsymbol{u}_d(t) = \left\{\frac{1}{2}\frac{\left[-4\omega_n r\dot{r} - \omega_n^2\left(r^2 - r^{\circ 2}\right)\right]}{r^2} - \frac{\dot{\boldsymbol{r}}\cdot\dot{\boldsymbol{r}}}{r^2}\right\}\boldsymbol{r} - \Delta\boldsymbol{f}$
$\frac{d^2(r^{-1})}{dt^2} \rightarrow$	$\boldsymbol{u}_d(t) = \left\{-r\left[2\omega_n\frac{\dot{r}}{r^2} - \omega_n^2\left(\frac{1}{r} - \frac{1}{r^\circ}\right)\right] - \frac{\dot{\boldsymbol{r}}\cdot\dot{\boldsymbol{r}}}{r^2}\right\}\boldsymbol{r} + 3\left(\frac{\dot{r}}{r}\right)\dot{\boldsymbol{r}} - \Delta\boldsymbol{f}$

variables to track the desired nominal values. For instance, let r° represent the nominal radial distance between the chief and deputy spacecraft and let r denote the actual radial distance between the vehicles. At any point in time, the actual radial distance may be determined from the relative position vector $\boldsymbol{r}$ as

$$r = \sqrt{\boldsymbol{r}^T\boldsymbol{r}} \tag{6}$$

Consider the scalar functions r, r^2, and $1/r$. Differentiating each of these expressions, until $\boldsymbol{u}_d(t)$ appears explicitly in the equations, leads—in each case—to one scalar second-order differential equation that depends on three unknown control inputs: the elements of $\boldsymbol{u}_d(t)$. Clearly, there are an infinite number of control accelerations that satisfy this scalar constraint. This indicates the existence of an optimal solution, although that is not the subject of the present investigation. To develop an understanding of the controlled phase space, Howell and Marchand[25] identify four particular solutions; the formation-keeping costs lead to a set of sample configurations. These results are summarized in Table 1. The first entry corresponds to a radial axis control law with zero transverse inputs. The remaining three entries are all subject to three-axis control. If the nominal relative separation between the vehicles is small, Howell and Marchand note that all four of these solutions appear to converge onto the same plane orbiting the chief spacecraft. However, in further studies[33,34] only three out of the four controllers, namely the three-axis control laws, are generally guaranteed to exhibit a planar response.

In fact, it can be shown analytically[34] that the plane of motion of the deputy vehicle, subject to any of these three control laws, is completely determined by the initial state of the vehicle at the time the controller is activated. It is also evident that, for each of these solutions, the controller forces the deputy vehicle to orbit the chief with some predetermined rate of rotation. The rate of rotation is determined by both the initial state and the controller formulation. This induced rotation rate can lead to prohibitively large formation-keeping costs, depending on the nominal relative separation between the vehicles. As the nominal relative distance decreases, the induced rotation rate increases and, thus, the associated formation-keeping costs increase as well. Because the dynamics tend to induce this rotation rate, the controller formulation is later extended, by Howell and Marchand,[33] to incorporate rotation rate control.

To illustrate the augmented controller formulation, note that the radial distance r can be differentiated twice to yield a scalar differential equation of the form

$$\ddot{r} = (\dot{\boldsymbol{r}}\cdot\dot{\boldsymbol{r}})/r + (\boldsymbol{r}\cdot\ddot{\boldsymbol{r}})/r - [(\boldsymbol{r}\cdot\dot{\boldsymbol{r}})/r^2]\dot{r} \tag{7}$$

Furthermore, observe that the forcing term $\Delta\boldsymbol{f}(\boldsymbol{r}, \boldsymbol{r}_c)$ and the control input $\boldsymbol{u}_d(t)$ appear explicitly in this expression through the acceleration term $\ddot{\boldsymbol{r}}$ defined in Eq. (2). Equation (7) may subsequently be reduced to the more compact form

$$\ddot{r} - r\dot{\theta}^2 = f_r + u_r \tag{8}$$

where $f_r = \Delta\boldsymbol{f}(\boldsymbol{r}, \boldsymbol{r}_c)\cdot\hat{\boldsymbol{r}}$, $u_r = \boldsymbol{u}_d(t)\cdot\hat{\boldsymbol{r}}$, and $\hat{\boldsymbol{r}} = \boldsymbol{r}/r$. The angular rate $\dot{\theta}$ describes the rate of rotation corresponding to an instantaneous orbit normal direction, $\hat{\boldsymbol{h}} = \boldsymbol{h}/h$, where $\boldsymbol{h} = \boldsymbol{r}\times\dot{\boldsymbol{r}}$ represents the angular momentum vector and $h = |\boldsymbol{h}|$ is its scalar magnitude. Let $\hat{\boldsymbol{\theta}} = \hat{\boldsymbol{h}}\times\hat{\boldsymbol{r}}$ such that $\hat{\boldsymbol{r}}$, $\hat{\boldsymbol{\theta}}$, and $\hat{\boldsymbol{h}}$ define an orthonormal triad. The instantaneous rotating coordinate system $\tilde{R}$, defined by $\hat{\boldsymbol{r}}$, $\hat{\boldsymbol{\theta}}$, and $\hat{\boldsymbol{h}}$, is not related to the rotating frame of the primaries, R. In the $\tilde{R}$ rotating coordinate system, the angular momentum vector is known to be of the form $\boldsymbol{h} = r^2\dot{\theta}\hat{\boldsymbol{h}}$. Differentiating the angular momentum vector with respect to time, as observed in the inertial frame, leads to one equation of constraint, $u_h + f_h = 0$, where $f_h = \Delta\boldsymbol{f}(\boldsymbol{r})\cdot\hat{\boldsymbol{h}}$ and $u_h = \boldsymbol{u}_d(t)\cdot\hat{\boldsymbol{h}}$. This operation further leads to one additional equation of motion,

$$r\ddot{\theta} + 2\dot{r}\dot{\theta} = f_\theta + u_\theta \tag{9}$$

where $f_\theta = \Delta\boldsymbol{f}(\boldsymbol{r}, \boldsymbol{r}_c)\cdot\hat{\boldsymbol{\theta}}$ and $u_\theta = \boldsymbol{u}_d(t)\cdot\hat{\boldsymbol{\theta}}$.

In this study, the nominal radial error dynamics are defined to follow a critically damped response, of natural frequency ω_n, such that the nominal radial response, $g_r(r, \dot{r})$, is determined as

$$\ddot{r} = g_r(r, \dot{r}) = \ddot{r}^\circ - 2\omega_n(\dot{r} - \dot{r}^\circ) - \omega_n^2(r - r^\circ) \tag{10}$$

The error dynamics for the rotation rate are then specified as a decaying exponential: $\delta\dot{\theta} = \delta\dot{\theta}(0)e^{-k\omega_n t}$. Subsequently, the nominal response $g_\theta(\dot{\theta})$ is then determined as

$$\ddot{\theta} = g_\theta(\dot{\theta}) = \ddot{\theta}^\circ - k\omega_n(\dot{\theta} - \dot{\theta}^\circ) \tag{11}$$

where k is an arbitrary scale factor and ω_n is the same natural frequency as in Eq. (10). Substitution of Eq. (11) into Eq. (9) and of Eq. (10) into Eq. (8) leads to the following scalar control laws:

$$u_r(t) = g_r(r, \dot{r}) - f_r - r\dot{\theta}^2 \tag{12}$$

$$u_\theta(t) = rg_\theta(\dot{\theta}) - f_\theta + 2\dot{r}\dot{\theta} \tag{13}$$

Constraint:

$$u_h(t) = -f_h \tag{14}$$

The control input that is actually applied to the deputy equations of motion, as listed in Eq. (2), is then determined by transforming the input vector described by Eqs. (12–14) back into the inertial frame:

$$\boldsymbol{u}_{D_i} = \{{}^I C^E\}[u_r \quad u_\theta \quad u_h]^T \tag{15}$$

where $\{{}^I C^E\} = [\hat{\boldsymbol{r}} \;\; \hat{\boldsymbol{\theta}} \;\; \hat{\boldsymbol{h}}]$

Application of Input/Output Feedback Linearization to Aspherical Formations

Interferometry missions are often envisioned in terms of vehicle arrangements that cannot be modeled as spherical. For instance, for MAXIM, the nominal path of the free-flyer vehicles may follow relative dynamics that are much different than that of the detector spacecraft, located thousands of kilometers aft of the free-flyer formation. This type of formation may best be modeled from the perspective of aspherical formation dynamics. To illustrate this concept, consider a multispacecraft formation where the deputy vehicles

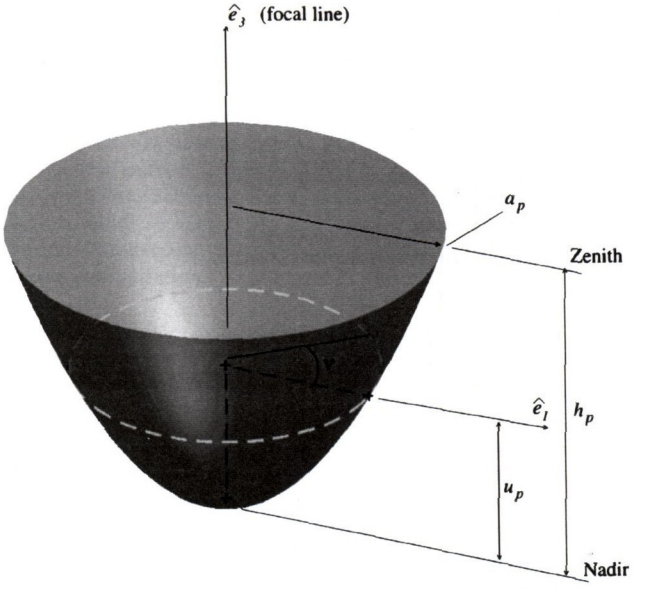

Fig. 3 Parameterization of a paraboloid.

evolve along an aspherical surface relative to the chief spacecraft. This surface is defined such that its orientation is inertially fixed. A paraboloid is an example of an aspherical surface and it is used as a proof of concept. In this particular example, the chief spacecraft and the nadir of the paraboloid define the focal line of the formation. Maintenance of a constant distance between the chief vehicle and the nadir of the paraboloid is the first objective of the controller. The second requirement is that the motion of all deputies, even during reconfigurations, is constrained to evolve along the surface of the paraboloid. To accomplish these goals, it is first necessary to define a suitable parameterization for the formation surface. To that end, consider the illustration in Fig. 3. The paraboloid in Fig. 3 is defined in an inertial frame (E) described in terms of the unit vectors $\hat{\boldsymbol{e}}_1$, $\hat{\boldsymbol{e}}_2$, and $\hat{\boldsymbol{e}}_3$.

The orientation of this frame, relative to the ephemeris inertial frame (I), is defined by the azimuth (α) and elevation (δ) of the focal line relative to the inertial (I) unit vectors $\hat{\boldsymbol{X}}$, $\hat{\boldsymbol{Y}}$, and $\hat{\boldsymbol{Z}}$. The "height" of any given deputy vehicle along this surface, measured relative to the nadir point, is defined by u_p, where $0 \le u_p \le h_p$ and h_p denotes the maximum allowable height along the paraboloid. The radius at the zenith of the paraboloid $(u_p = h_p)$ is denoted by the variable a_p. The unit vector $\hat{\boldsymbol{e}}_1$, defined as $\hat{\boldsymbol{e}}_1 = \hat{\boldsymbol{Z}} \times \hat{\boldsymbol{e}}_3 / |\hat{\boldsymbol{Z}} \times \hat{\boldsymbol{e}}_3|$, is simply a reference direction for the measurement of the angular position (ν) along the surface in Fig. 3. Of course, $\hat{\boldsymbol{e}}_2 = \hat{\boldsymbol{e}}_3 \times \hat{\boldsymbol{e}}_1$ completes the right-handed inertial triad. The variables ν and u_p completely specify the position of a deputy vehicle along the formation surface in Fig. 3. The paraboloid itself is offset from the chief vehicle by a distance $q(t)$ along the $\hat{\boldsymbol{e}}_3$ axis.

A parabolic configuration requires the tracking of three variables: $u_p(t)$, $q(t)$, and $\dot{\nu}(t)$. To illustrate how an OFL controller may be applied to this type of configuration, it is necessary to establish a set of expressions relating the state variables (and control inputs) to the tracked quantities. For instance, recall that

$$\boldsymbol{\rho}_E = \{{}^E C^I\}\boldsymbol{\rho}_I = [\tilde{x} \quad \tilde{y} \quad \tilde{z}]^T \tag{16}$$

where the tilde above each variable indicates that the measure numbers are associated with the focal frame (E) of the paraboloid. These measure numbers are related to the paraboloid parameters in Fig. 3 as follows:

$$\tilde{x} = a_p \sqrt{u_p / h_p} \cos \nu \tag{17}$$

$$\tilde{y} = a_p \sqrt{u_p / h_p} \sin \nu \tag{18}$$

$$\tilde{z} = q + u_p \tag{19}$$

Note that it is possible to explicitly solve for u_p, ν, and q by algebraic manipulation of Eqs. (17–19). Consistent with the OFL approach, the resulting expressions may be differentiated twice with respect to time until the elements of the control acceleration vector appear explicitly. Differentiation is straightforward and ultimately suggests that

$$g_{u_p}(u_p, \dot{u}_p) - \frac{2h_p}{a_p^2}\left(\dot{\tilde{x}}^2 + \dot{\tilde{y}}^2 + \tilde{x}\Delta\tilde{f}_x + \tilde{y}\Delta\tilde{f}_y\right) = \frac{2h_p}{a_p^2}\tilde{x}\tilde{u}_x + \frac{2h_p}{a_p^2}\tilde{y}\tilde{u}_y \tag{20}$$

$$g_q(q, \dot{q}) + \frac{2h_p}{a_p^2}\left(\dot{\tilde{x}}^2 + \dot{\tilde{y}}^2 + \tilde{x}\Delta\tilde{f}_x + \tilde{y}\Delta\tilde{f}_y\right) - \Delta\tilde{f}_z = -\frac{2h_p}{a_p^2}\tilde{x}\tilde{u}_x - \frac{2h_p}{a_p^2}\tilde{y}\tilde{u}_y + \tilde{u}_z \tag{21}$$

$$g_{\dot{\nu}}(\dot{\nu}) + 2\frac{(\tilde{x}\dot{\tilde{x}} + \tilde{y}\dot{\tilde{y}})(\tilde{x}\dot{\tilde{y}} - \tilde{y}\dot{\tilde{x}})}{(\tilde{x}^2 + \tilde{y}^2)^2} + \frac{(\tilde{y}\Delta\tilde{f}_x - \tilde{x}\Delta\tilde{f}_y)}{(\tilde{x}^2 + \tilde{y}^2)} = \frac{\tilde{x}}{(\tilde{x}^2 + \tilde{y}^2)}\tilde{u}_y - \frac{\tilde{y}}{(\tilde{x}^2 + \tilde{y}^2)}\tilde{u}_x \tag{22}$$

In Eqs. (20–22), recall that the tilde represents quantities associated with the focal frame (E) of the paraboloid. Hence, $\tilde{u}_x$, $\tilde{u}_y$, and $\tilde{u}_z$ are the components of $\tilde{\boldsymbol{u}} = \{{}^E C^I\}\boldsymbol{u}$, the transformed control input vector. Similarly, $\Delta\tilde{f}_x$, $\Delta\tilde{f}_y$, and $\Delta\tilde{f}_z$ are the elements of $\Delta\tilde{\boldsymbol{f}} = \{{}^E C^I\}\Delta\boldsymbol{f}^{(D_i)}$. The scalar functions $g_{u_p}(u_p, \dot{u}_p)$, $g_q(q, \dot{q})$, and $g_{\dot{\nu}}(\dot{\nu})$ reflect the desired dynamic response for the variables u_p, q, and $\dot{\nu}$. As an example, critically damped error dynamics, of frequency ω_n, are desired for the distance elements u_p and q whereas an exponentially decaying error response is sought for $\dot{\nu}$.

An exact solution is available for Eqs. (20–22). To simplify the form of the solution, let $\alpha_x = 2h_p\tilde{x}/a_p^2$, $\alpha_y = 2h_p\tilde{y}/a_p^2$, $\beta_x = \tilde{x}/(\tilde{x}^2 + \tilde{y}^2)$, and $\beta_y = \tilde{y}/(\tilde{x}^2 + \tilde{y}^2)$. Furthermore, let the left-hand side of Eqs. (20–22) be summarized by G_{u_p}, G_q, and $G_{\dot{\nu}}$, respectively. Then the commanded control input is expressed:

$$\tilde{u}_x = \frac{\left(\beta_x G_{u_p} - \alpha_y G_{\dot{\nu}}\right)}{(\alpha_x\beta_x + \alpha_y\beta_y)} \tag{23}$$

$$\tilde{u}_y = \frac{\left(\beta_y G_{u_p} + \alpha_x G_{\dot{\nu}}\right)}{(\beta_x\alpha_x + \beta_y\alpha_y)} \tag{24}$$

$$\tilde{u}_z = G_{u_p} + G_q \tag{25}$$

Note that the preceding control law is singular if the deputy crosses the focal line $(\hat{\boldsymbol{e}}_3)$, $\tilde{x} = \tilde{y} = 0$. This does not present a significant issue, however, because once the deputy is on the surface of the paraboloid this condition is never met. This singularity can only occur while the deputy is being driven onto the surface during the injection phase. To circumvent this difficulty, it is only necessary to allow the vehicle to coast away from this point before reactivating the controller. For implementation of this approach in the ephemeris model, the integration of each vehicle proceeds separately in an Earth-centered inertial frame I. The relative state of the deputy with respect to the chief is computed from these Earth-centered states. These quantities are then transformed into the focal frame (E) via $\tilde{\boldsymbol{r}} = \{{}^E C^I\}\boldsymbol{r}$ and $\dot{\tilde{\boldsymbol{r}}} = \{{}^E C^I\}\dot{\boldsymbol{r}}$. The results of this transformation are substituted into Eqs. (17–19) and the values of u_p, ν, and q are subsequently determined. Finally, the necessary control accelerations are computed from Eqs. (23–25).

Results

Recall that, throughout this study, the chief spacecraft is assumed to evolve along an unstable orbit near the libration points. It is further assumed that the desired baseline motion of the deputy vehicle does

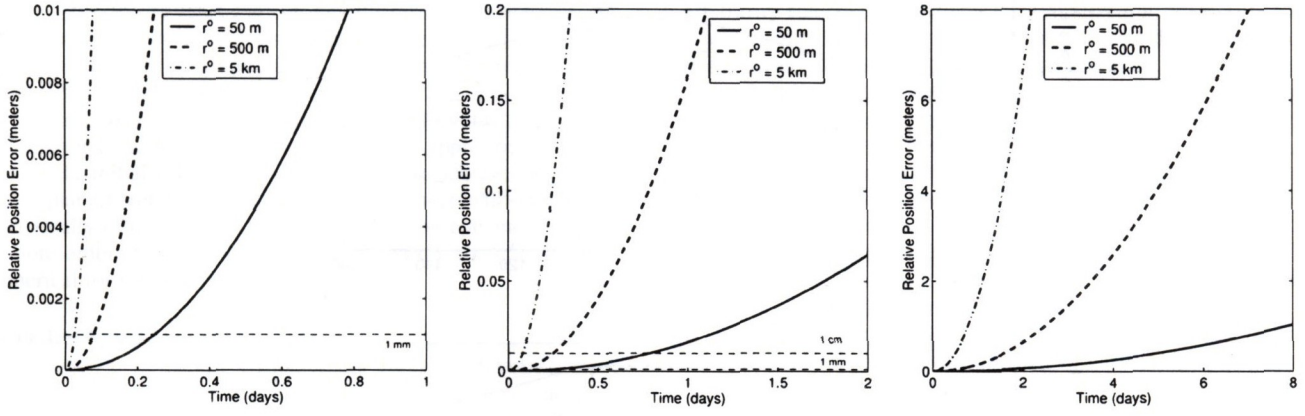

Fig. 4 Growth in nominal relative separation for a sample uncontrolled formation.

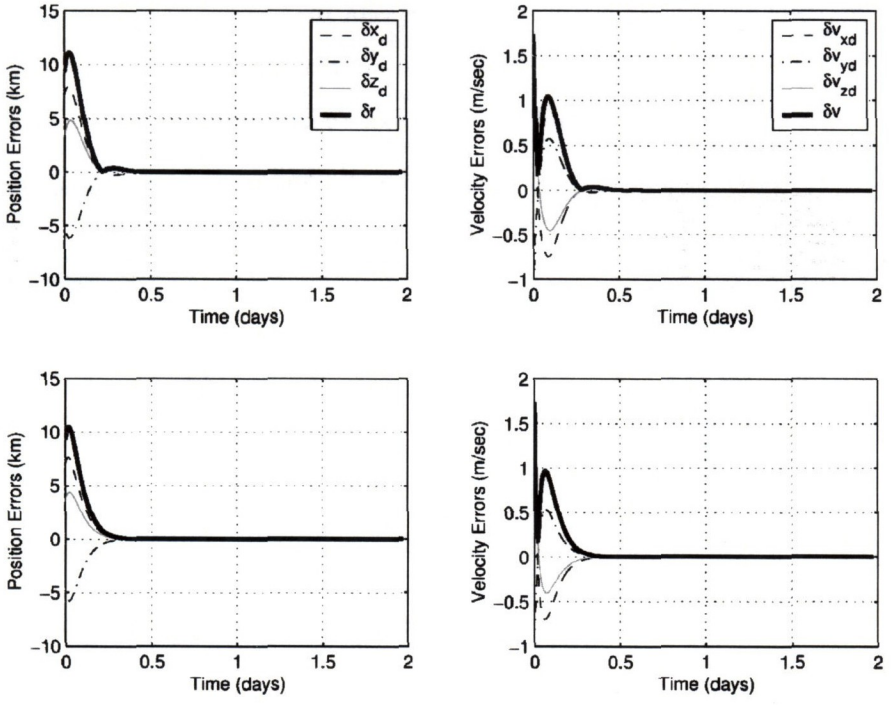

Fig. 5 Sample LQR vs IFL error response for deputy spacecraft in a 5000-km formation, fixed relative to the rotating frame (over 6 months), Near a 200,000-km L_1 halo orbit.

not correspond to a naturally occurring solution. Hence, if left uncontrolled, the deputy may quickly depart the vicinity of the chief spacecraft as it evolves along its path. To illustrate this, suppose that the chief spacecraft is known to evolve along a halo orbit with out-of-plane amplitude A_z of 200,000 km. Define a sample nominal formation where the deputy spacecraft remains at a constant relative distance from the chief vehicle. This nominal separation ranges between $r^\circ = 50$ m and $r^\circ = 5$ km. The nominal relative radial vector is assumed to be of the form $\boldsymbol{r}^\circ(t) = r^\circ \hat{\mathbf{y}}$. Thus, the orientation of the chief–deputy radial line is fixed relative to the rotating frame, ${}^R\dot{\boldsymbol{r}} = \mathbf{0}$ m/s. In the immediate vicinity of the reference halo orbit, the relative position error, given by $|\boldsymbol{r} - \boldsymbol{r}^\circ|$, appears to grow quadratically with time, as evidenced from Fig. 4.

For a 50-m relative separation, and in the absence of control inputs, the natural response of the system places the deputy anywhere above the 1-mm error mark within 6 h, 1 cm within 18 h, and 1 m within 8 days. If, instead, the nominal separation is 5 km, the deputy crosses the 1-mm error mark within 35 min, the 1-cm mark in just under 2 h, and the 1-m mark in almost 20 h. This suggests that, if the formation tolerances are not too constrained, a discrete control approach may be sufficient for small formations. However, if the configuration constraints require submillimeter accuracy at all times, nearly continuous control is necessary. For missions like MAXIM, in which the detector spacecraft may be as far as 20,000 km away, this is of great significance.

Fixed-State Formation Control: Comparison of ILF and LQR Methodologies

LQR and input-state feedback linearization methods are applied here to a 5000-km two-spacecraft formation fixed relative to the rotating frame as defined in the CR3BP. Note that both methods can be successfully applied to either the chief spacecraft orbit or the deputy dynamics in either the CR3BP or the ephemeris model for any type of formation. In this example, the line defining the formation is commanded to track the rotating y axis at all times. Consistent with Fig. 2, this type of formation represents the most cost effective baseline configuration. Figure 5 illustrates the response to an injection error defined by $\boldsymbol{e}(0) = (7, -5, 3.5)$ km and $\dot{\boldsymbol{e}}(0) = (1, -1, 1)$ m/s. The top two plots in Fig. 5 illustrate the response of the error dynamics in each state to the LQR controller, for a particular set of state error and control input weighting matrices, Q and R. In contrast, the two plots at the bottom of Fig. 5 illustrate the error response corresponding to each state for a controller based on the IFL approach, as represented by Eq. (5), for $\omega_n = 1250$. Note that, in this example, both controllers yield good tracking characteristics at essentially the same cost, as illustrated in Fig. 6. The two time histories illustrated

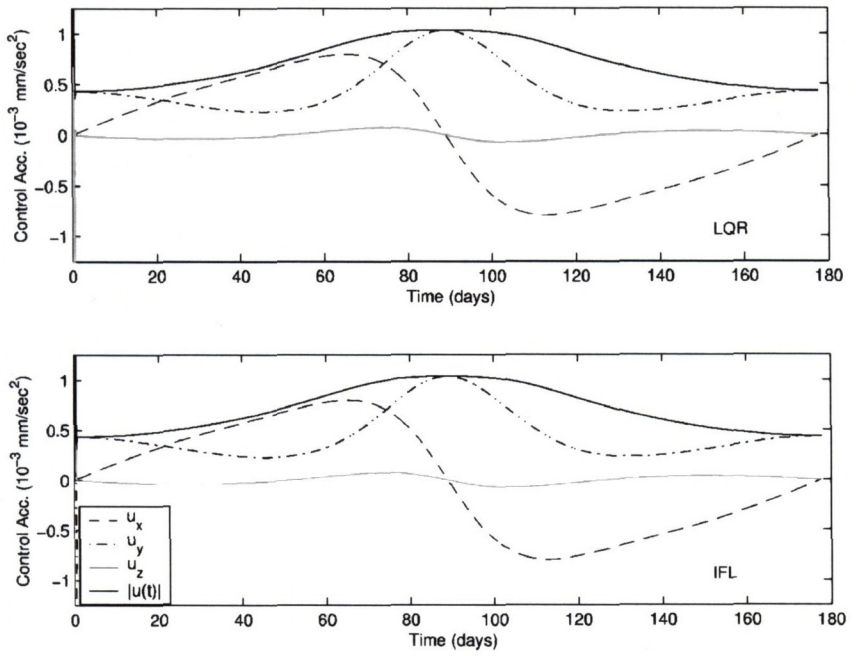

Fig. 6 LQR vs IFL control accelerations for deputy spacecraft in a 5000-km formation, fixed relative to the rotating frame (over 6 months), near a 200,000-km L_1 halo orbit.

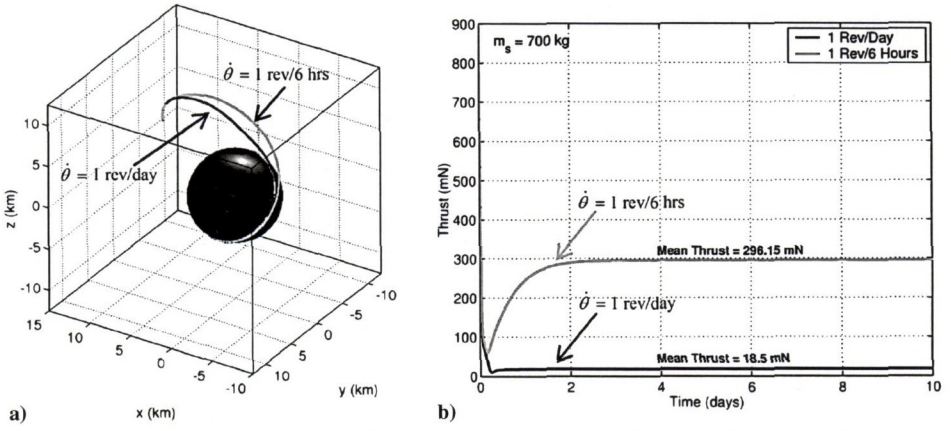

Fig. 7 OFL control of radial distance plus rotation rate and associated thrust profile.

in this figure represent a close-up view of the converged control acceleration components and of the associated net magnitude, beyond the injection phase.

Observe that, for a 5000-km nominal separation and a 1000-kg deputy vehicle, the thrust level required to enforce the desired configuration is, roughly, between 0.5 and 1.0 mN. This is consistent with the results previously presented in Fig. 2. Also, although the results in Fig. 5 reflect only the response to initial injection errors, the methodology is easily extended to formation reconfigurations simply by redefining the nominal path appropriately at the desired times.

In comparing the LQR and IFL results, the following information is notable. Clearly, it is possible to identify error weighting matrices such that the LQR and IFL responses are *nearly* identical. However, the selection of the elements of these matrices is not necessarily trivial. In fact, the selection itself can be envisioned as an optimization problem. The goal of the preceding example is to obtain a very specific set of response characteristics. In the IFL analysis, a critically damped response is sought. Matching the LQR response to that of the IFL controller requires a very specific set of position and velocity weights. The appropriate ratio between the position and velocity weights is determined experimentally. The IFL approach eliminates the need for this determination and, thus, is simpler for the preliminary cost estimate.

Radial Distance and Rotation Rate Tracking

Consider a sample formation where the chief spacecraft evolves along a Lissajous trajectory, as determined in the ephemeris model. This quasi-periodic trajectory resembles the halo orbit used in the two earlier examples. Let the nominal motion be defined by a relative separation of 5 km between the chief and deputy vehicles. To illustrate the impact of the rotation rate on the formation-keeping cost, consider two examples characterized by $\dot{\theta} = 1$ revolutions/day and $\dot{\theta} = 1$ revolution/6 h. A sample implementation of the control law in Eq. (15) is illustrated in Fig. 7 for a 700-kg spacecraft. In Fig. 7a, the relative initial state is defined by $\boldsymbol{r}(0) = [12 \;\; -5 \;\; 3]$ km and $\dot{\boldsymbol{r}}(0) = [1 \;\; -1 \;\; 1]$ m/s.

The equation of constraint in Eq. (14) guarantees that the plane of motion is completely determined by the relative state of the deputy before the controller is activated. From Fig. 8, it is also apparent that the formation-keeping cost increases quadratically with rotation rate and linearly with the separation that is commanded between the chief and deputy vehicles. In this figure, cost is represented in terms of the mean thrust level that is required to enforce the nominal solution over the duration of the mission (180 days), assuming the vehicle mass is 700 kg.

For a nominal separation of 50 m, commanding the deputy to spin at one revolution per hour, about the chief spacecraft, requires over 100 mN of thrust for a 700-kg vehicle. The mean thrust drops to

6.7 mN if the deputy vehicle is to nominally orbit the chief spacecraft once every 4 h. The thrust levels continue to drop to 0.19 mN for one revolution per day. If one revolution per day is required, a 500-m separation raises the mean thrust to 18 mN.

Although the plane of motion is not affected by this type of control approach, activating the controller at the appropriate time, or biasing the initial velocity, may be sufficient to achieve the desired orbital plane. Overall, the control strategy is conceptually simple and numerically efficient for implementation in the ephemeris model. A more ambitious goal involving OFL control, then, is to target aspherical formations.

Aspherical Formation Control

Consider a formation characterized by $\boldsymbol{q} = (10\,\text{km})\hat{\boldsymbol{e}}_3$, $h_p = 500$ m, and $a_p = 500$ m. Let the focal line be oriented such that $\alpha = 0$ deg and $\delta = 45$ deg. Each vehicle in the formation is to complete one revolution along the surface once per day: $\dot{\nu} = 1$ revolution/day. The nominal motion of one of the vehicles is initially described by $u_p = 200$ m such that $\dot{u}_p = \ddot{u}_p = 0$ and $\ddot{\nu} = 0$. After 5 days, the vehicle's nominal path must be reconfigured, along the paraboloid, such that $\dot{\nu}$ and $\dot{u}_p$ remain constant. The climb rate $\dot{u}_p$ is specified such that, after 1 day, the vehicle has raised its "height" to 500 m relative to the nadir of the paraboloid, a 300-m climb relative to the initial orbit. Let the initial relative state of the deputy vehicle be defined such that $\boldsymbol{r}(0) = (4.6\hat{\boldsymbol{X}} + 4.3\hat{\boldsymbol{Y}} + 6.934\hat{\boldsymbol{Z}})$ km and $\dot{\boldsymbol{r}}(0) = 0.05\hat{\boldsymbol{X}} - 0.05\hat{\boldsymbol{Y}} - 0.05\hat{\boldsymbol{Z}}$ m/s. This particular initial state is arbitrarily selected to facilitate the visualization process. For any arbitrary initial state, the controller should first drive the vehicles in the formation to the initial target configuration, then reconfigure at the appropriate time. Once deployed, this evolution is to proceed along the surface of the paraboloid. Application of this controller results in the trajectory illustrated in Fig. 9.

The resulting path is divided into three segments. The segment highlighted in orange represents the injection phase as well as the initial orbit phase, for $u_p = 200$ m. The green segment denotes the reconfiguration phase, characterized by $\dot{u}_p = 300$ m/day. The last segment, in blue, is the final phase associated with $u_p = 500$ m. The thrust profile associated with this solution appears in Fig. 10.

According to Fig. 10, the thrust levels for a 700-kg deputy vehicle range between 25 mN during injection to 1–2 mN for orbit maintenance. The 1–2 mN represents the nominal formation-keeping cost required to track the desired path. Note that the maximum thrust amplitude will vary according to the response frequency specified for the variables u_p, q, and $\dot{\nu}$. Also, although both the nominal and actual thrust profiles appear to converge onto constant segments, there is an oscillation on the order of 0.003 mN during the orbit phase at $u_p = 200$ m (last part of phase 1) and $u_p = 500$ m (phase 3), that is, assuming the deputy mass is 700 kg.

Although the overall configurations may appear different, spherical and aspherical configurations share one thing in common: in both cases, fuel expenditure is most heavily influenced by induced relative rotations rather than relative separation. Hence, for parabolic formations, cost still increases quadratically with rotation rate along

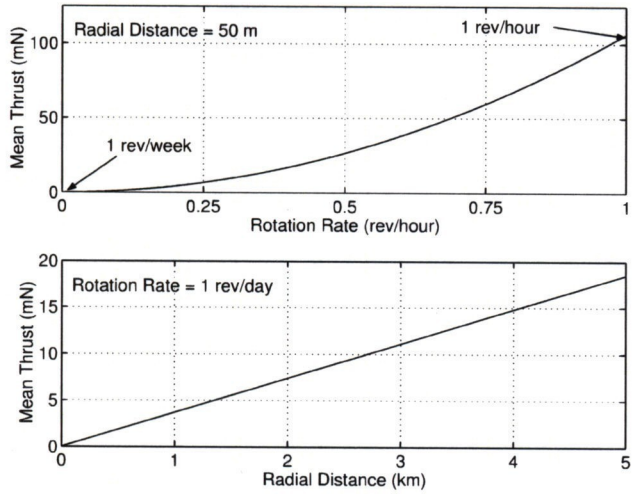

Fig. 8 Impact of commanded radial distance and spin rate on formation-keeping costs.

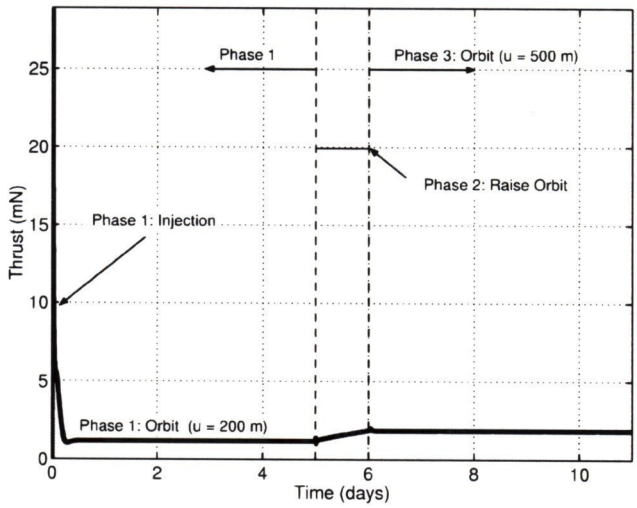

Fig. 10 Thrust profile for OFL controlled parabolic formation.

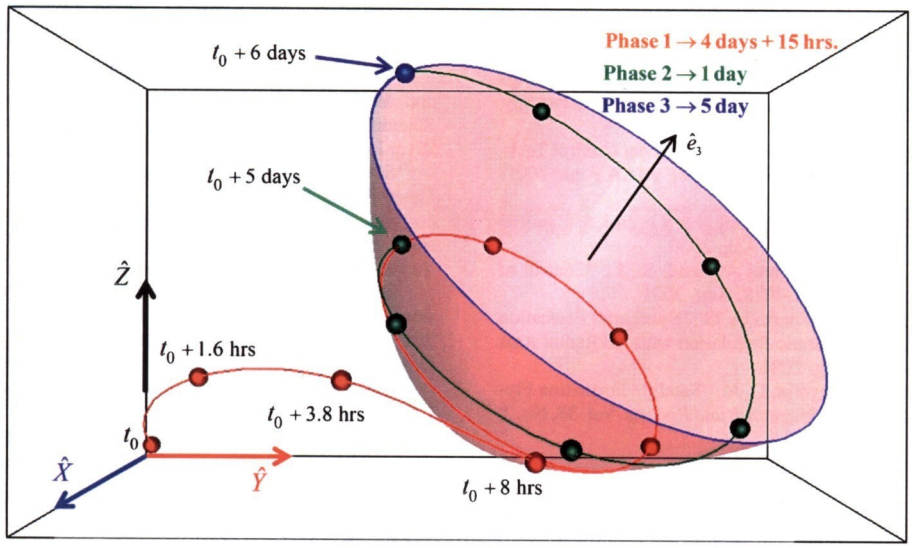

Fig. 9 OFL controlled parabolic formation.

the surface and linearly with relative vehicle separation with respect to the chief spacecraft.

Conclusions

In the present investigation, optimal control and feedback linearization techniques are successfully applied to deploy, enforce, and reconfigure a variety of formation configurations near the vicinity of the libration points of the SEM system. Although the CR3BP serves as an accurate initial guess for preliminary analysis, all the control laws considered are ultimately implemented in the full ephemeris model. The ephemeris model analysis can include solar radiation pressure and any number of desired gravitational perturbations. Depending on the constraints imposed on the formation, the results presented in this study can require thrust levels anywhere on the order of nano- to milli-Newtons, for a 700–1000-kg spacecraft. In contrast, the deployment phase can require thrust levels in the Newton range, depending on when the controller is activated. Even if the formation constraints can be met, theoretically, the sensitivity of these methods to modeling and thruster implementation errors must be addressed. This is of particular importance for libration point missions given the associated dynamic sensitivities to small perturbations. Certainly, for any of the examples presented here, discontinuing the thrust input at any time, or placing bounds on its amplitude, leads to divergence from the desired nominal, especially with the higher rates of rotation that induce higher tangential speeds.

Acknowledgments

This research was carried out at Purdue University with support from the Clare Boothe Luce Foundation. It was also funded under Cooperative Agreement NCC5-727 through the NASA Goddard Space Flight Center Formation Flying NASA Research Announcement. The authors thank Mario Rotea for valuable discussions. Any opinions, findings, and conclusions or recommendations expressed in this material are those of the authors and do not necessarily reflect the views of NASA.

References

[1]Vassar, R. H., and Sherwood, R. B., "Formationkeeping for a Pair of Satellites in a Circular Orbit," *Journal of Guidance, Control, and Dynamics*, Vol. 8, No. 2, 1985, pp. 235–242.

[2]Redding, D. C., Adams, N. J., and Kubiak, E. T., "Linear-Quadratic Stationkeeping for the STS Orbiter," *Journal of Guidance, Control, and Dynamics*, Vol. 12, No. 2, 1989, pp. 248–255.

[3]Ulybyshev, Y., "Long-Term Formation Keeping of Satellite Constellation Using Linear Quadratic Controller," *Journal of Guidance, Control, and Dynamics*, Vol. 21, No. 1, 1998, pp. 109–115.

[4]Kapila, V., Sparks, A. G., Buffington, J. M., and Yan, Q., "Spacecraft Formation Flying: Dynamics and Control," *Journal of Guidance, Control, and Dynamics*, Vol. 23, No. 3, 2000, pp. 561–563.

[5]Sparks, A., "Satellite Formationkeeping Control in the Presence of Gravity Perturbations," *Proceedings of the American Control Conference*, Vol. 2, IEEE Publications, Piscataway, NJ, 2000, pp. 844–848.

[6]Yedavalli, R. K., and Sparks, A. G., "Satellite Formation Flying Control Design Based on Hybrid Control System Stability Analysis," *Proceedings of the American Control Conference*, Vol. 3, IEEE Publications, Piscataway, NJ, 2000, pp. 2210–2214.

[7]Irvin, D. J., Jr., and Jacques, D. R., "Linear vs. Nonlinear Control Techniques for the Reconfiguration of Satellite Formations," AIAA Paper 2001-4089, Aug. 2001.

[8]Stansbery, D. T., and Cloutier, J. R., "Nonlinear Control of Satellite Formation Flight," AIAA Paper 2000-4436, Aug. 2000.

[9]Vadali, S. R., Vaddi, S. S., Naik, K., and Alfriend, K. T., "Control of Satellite Formations," AIAA Paper 2001-4028, Aug. 2001.

[10]Starin, S. R., Yedavalli, R. K., and Sparks, A. G., "Spacecraft Formation Flying Maneuvers Using Linear Quadratic Regulation with No Radial Axis Inputs," AIAA Paper 2001-4029, Aug. 2001.

[11]Sabol, C., Burns, R., and McLaughlin, C. A., "Satellite Formation Flying Design and Evolution," *Journal of Spacecraft and Rockets*, Vol. 38, No. 2, 2001, pp. 270–278.

[12]Chao, C. C., Pollard, J. E., and Janson, S. W., "Dynamics and Control of Cluster Orbits for Distributed Space Missions," American Astronautical Society, Paper 99-126, Feb. 1999.

[13]Schaub, H., and Alfriend, K. T., "Impulsive Spacecraft Formation Flying Control to Establish Specific Mean Orbit Elements," *Journal of Guidance, Control, and Dynamics*, Vol. 24, No. 4, 2001, pp. 739–745.

[14]Tan, Z., Bainum, P. M., and Strong, A., "The Implementation of Maintaining Constant Distance Between Satellites in Elliptic Orbits," *Advances in the Astronautical Sciences*, Vol. 105, Jan. 2000, pp. 667–683.

[15]Wang, Z., Khorrami, F., and Grossman, W., "Robust Adaptive Control of Satellite Formationkeeping for a Pair of Satellites," *Proceedings of the American Control Conference*, Vol. 2, IEEE Publications, Piscataway, NJ, 2000, pp. 834–838.

[16]de Queiroz, M. S., Kapila, V., and Yan, Q., "Adaptive Nonlinear Control of Multiple S/C Formation Flying," *Journal of Guidance, Control, and Dynamics*, Vol. 23, No. 3, 2000, pp. 385–390.

[17]Yan, Q., Yang, G., Kapila, V., and de Queiroz, M. S., "Nonlinear Dynamics and Output Feedback Control of Multiple Spacecraft in Elliptic Orbit," *Proceedings of the American Control Conference*, Vol. 2, IEEE Publications, Piscataway, NJ, 2000, pp. 839–843.

[18]Scheeres, D. J., and Vinh, N. X., "Dynamics and Control of Relative Motion in an Unstable Orbit," AIAA Paper 2000-4135, Aug. 2000.

[19]TPF Science Working Group, "The Terrestrial Planet Finder (TPF): A NASA Origins Program to Search for Habitable Planets," Jet Propulsion Lab. Publ. 99-003 [online], URL: http://planetquest.jpl.nasa.gov/TPF/tpf_book/[cited May 1999].

[20]Hamilton, N. H., "Formation Flying Satellite Control Around the L_2 Sun–Earth Libration Point," M.S. Thesis, School of Engineering and Applied Science, George Washington Univ., Washington, DC, Dec. 2001.

[21]Folta, D., Carpenter, J. R., and Wagner, C., "Formation Flying with Decentralized Control in Libration Point Orbits," *International Symposium: Spaceflight Dynamics*, Biarritz, France, June 2000.

[22]Barden, B. T., and Howell, K. C., "Fundamental Motions near Collinear Libration Points and Their Transitions," *Journal of Astronautical Sciences*, Vol. 46, No. 4, 1998, pp. 361–378.

[23]Barden, B. T., and Howell, K. C., "Formation Flying in the Vicinity of Libration Point Orbits," *Advances in Astronautical Sciences*, Vol. 99, Pt. 2, 1998, pp. 969–988.

[24]Howell, K. C., and Barden, B. T., "Trajectory Design and Stationkeeping for Multiple Spacecraft in Formation near the Sun–Earth L_1 Point," International Astronautical Federation/International Academy of Astronautics Congress, IAF/IAA Paper 99-A707, Amsterdam, Oct. 1999.

[25]Howell, K. C., and Marchand, B. G., "Natural and Non-Natural Spacecraft Formations near the L_1 and L_2 Libration Points in the Sun–Earth/Moon Ephemeris System," *Dynamical Systems: An International Journal, Special Issue:* Dynamical Systems in Dynamical Astronomy and Space Mission Design, Vol. 20, No. 1, 2005, pp. 149–173.

[26]Gómez, G., Lo, M., Masdemont, J., and Museth, K., "Simulation of Formation Flight near Lagrange Points for the TPF Mission," American Astronautical Society, Paper 01-305, July 2001.

[27]Mueller, J., "Thruster Options for Microspacecraft: A Review and Evaluation of Existing Hardware and Emerging Technologies," AIAA Paper 97-3058, July 1997.

[28]Gonzales, A. D., and Baker, R. P., "Microchip Laser Propulsion for Small Satellites," AIAA Paper 2001-3789, July 2001.

[29]Phipps, C., and Luke, J., "Diode Laser-Driven Microthrusters—A New Departure for Micropropulsion," *AIAA Journal*, Vol. 40, No. 2, 2002, pp. 310–318.

[30]Chen, G., Fang, J., Hong, Y., and Qin, H., "Introduction to Chaos Control and Anti-Control," *Advanced Topics in Nonlinear Control Systems*, World Scientific Series on Nonlinear Science, Ser. A, Vol. 40, World Scientific, River Edge, NJ, 2001, pp. 193–245.

[31]Slotine, J. E., and Li, W., *Applied Nonlinear Control*, Prentice–Hall, Upper Saddle River, NJ, 1991.

[32]Howell, K. C., and Marchand, B. G., "Control Strategies for Formation Flight in the Vicinity of the Libration Points," American Astronautical Society, Paper 03-113, Feb. 2003.

[33]Howell, K. C., and Marchand, B. G., "Design and Control of Formations near the Libration Points of the Sun–Earth/Moon Ephemeris System," 2003 Space Flight Mechanics Symposium, Goddard Space Flight Center. Greenbelt, Maryland, Oct. 2003.

[34]Marchand, B. G., and Howell, K. C., "Aspherical Formations near the Libration Points of the Sun–Earth/Moon System," American Astronautical Society, Paper 04-157, Feb. 2004.